Enhanced Backscattering Optical Fiber Distributed Sensors: Tutorial and Review

Daniele Tosi, Carlo Molardi, Marzhan Sypabekova, Wilfried Blanc

Enhanced Backscattering Optical Fiber Distributed Sensors: Tutorial and Review

Daniele Tosi, Carlo Molardi, *Member, IEEE*, Marzhan Sypabekova, and Wilfried Blanc

***Abstract*—Optical Backscatter Reflectometry (OBR) is an advanced distributed sensing technique that makes use of optical fibers to detect and localize physical parameters, with spatial resolution below the millimeter. By tailoring the Rayleigh scattering properties of optical fibers, enhancing the backscattering contents, we can create 2 and 3-dimensional sensing networks that can extend OBR to multi-dimensional sensing, and even to biosensing. In this work, we provide a tutorial on distributed optical fiber sensors with enhanced backscattering, and on how to design sensing networks with these fibers; we also review the main applications and emerging topics.**

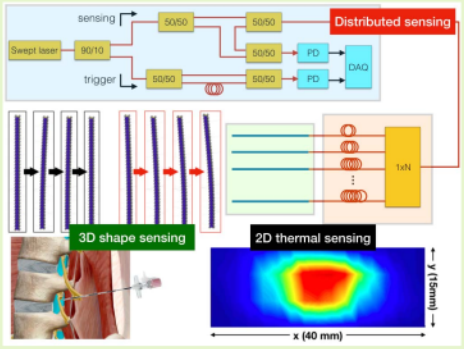

***Index Terms*— Optical fiber sensors, distributed sensors, Rayleigh scattering, optical backscattering reflectometry, optical fiber biosensors.**

I. Introduction

DISTRIBUTED optical fiber sensors have been established during the last two decades [1]–[6], and represent a unique sensing technology capable of resolving mechanical or physical parameters through each point of an optical fiber. This key property allows fast and spatially resolved measurement of temperature [7], [8], strain [9], [10], shape [11], [12], humidity [13], sound pressure waves [14], [15] in-line into an optical fiber, making it a unique technology unmatched by other electrical, electronic, or electro-mechanical sensors. Within this field, optical time-domain reflectrometry (OTDR) methods have been preferred for their capability of detecting over long distances [16], [17], with the recent advent of phase-OTDR (φ-OTDR) for low spatial resolution sensing [9], [18]. On the other hand, optical frequency-domain reflectometry (OFDR) techniques have been implemented for sub-centimeter sensing [8], [19], [20]. Optical backscatter reflectometry (OBR) is the most modern and popular OFDR method [6], [21], [22].

The key concept of distributed sensors is to interrogate the multiple weak reflections occurring into each point of an optical fiber, as the light waves travels through each portion of the fiber link. Weak reflections can be induced by inscribing weak gratings into the fiber [5], [19], or random optical gratings [23]. However, even in absence of any microfabricated device, Rayleigh scattering into the fiber provides the ultimate reflectivity term that we can interrogate; this is the concept at the base of OBR [21].

The optical fibers used in sensing are mainly derived from telecommunications; their characteristics are well standardized by ITU-T Recommendation G.652.D [24]. Since Rayleigh scattering is a loss factor in optical fibers, the need for long-haul communication links has pushed researchers to engineer

Manuscript received June 26, 2020; revised July 17, 2020; accepted July 17, 2020. Date of publication July 20, 2020; date of current version May 28, 2021. This work was supported in part by Nazarbayev University (SMARTER and EPICGuide) under Grant 091019CRP2117 and Grant 240919FD3908 and in part by the ANR Project NanoSlim under Grant ANR-17-CE08-0002. The associate editor coordinating the review of this article and approving it for publication was Dr. Carlos Marques. *(Corresponding author: Daniele Tosi.)*

Daniele Tosi is with the School of Engineering and Digital Sciences, Nazarbayev University, Nur-Sultan 010000, Kazakhstan, also with the National Laboratory Astana, Nazarbayev University, Nur-Sultan 010000, Kazakhstan, and also with the Laboratory of Biosensors and Bioinstruments, Nazarbayev University, Nur-Sultan 010000, Kazakhstan (e-mail: daniele.tosi@nu.edu.kz).

Carlo Molardi is with the School of Engineering and Digital Sciences, Nazarbayev University, Nur-Sultan 010000, Kazakhstan (e-mail: carlo.molardi@nu.edu.kz).

Marzhan Sypabekova is with the School of Medicine, Nazarbayev University, Nur-Sultan 010000, Kazakhstan, also with the National Laboratory Astana, Nazarbayev University, Nur-Sultan 010000, Kazakhstan, and also with the Laboratory of Biosensors and Bioinstruments, Nazarbayev University, Nur-Sultan 010000, Kazakhstan (e-mail: msypabekova@nu.edu.kz).

Wilfried Blanc is with the Centre National de la Recherche Scientifique (CNRS), INPHYNI, UMR 7010, Université Côte d'Azur, 06108 Nice, France (e-mail: wilfried.blanc@inphyni.cnrs.fr).

Digital Object Identifier 10.1109/JSEN.2020.3010572

fabrication methods that could lower the fiber attenuation down to the theoretical limit for Rayleigh scattering [25]. In an OBR configuration, the Rayleigh scattering corresponds to the amount of light reflected back to the detector, hence by minimizing the scattering content we obtain the minimum power at the photodetector; however, modern OBR systems such as [6] can handle the OBR detection even with such low power values.

Recently, several research centers have however tried to reverse the trend: increasing the Rayleigh scattering to create enhanced backscattering fibers (EBFs), which have significantly higher scattering content [26]–[37]. The best results have been achieved by means of fibers doped with MgO-based nanoparticles (MgO-NP) within the core, which can be handled like standard fibers [26]–[32]. The advantage of EBFs in lieu of standard fibers is not only limited to improving the signal-to-noise ratio [36], but with a proper arrangement it is possible to generate a new multiplexing domain labelled scattering-level multiplexing (SLMux) [38], which allows a simultaneous detection of multiple fibers. Several recent works have reported excellent results of SLMux in 2D/3D sensing of tens of fibers [28]–[30], as well as extending sensing to refractive index and biological parameters [26], [27], [31].

This work provides a tutorial for engineers, scientists, and optical fiber specialists on distributed sensing with EBF, and reviews the recent applications. The structure is the following: Sect. II provides the general design of a OBR-SLMux network; Sect. III provides the theoretical considerations; Sect. IV describes the fabrication and characterization of MgO-NP fibers and other scattering enhancement methods; Sect. V reviews the OBR-SLMux applications with particular emphasis on the biomedical scenarios; finally, in Sect. VI conclusions are drawn.

II. OBR Sensing Networks and Multiplexing

The general design of an OBR sensing network, which uses fibers with enhanced backscattering, is shown in Fig. 1 [38]; while the OBR is generally a single-channel system [6], which can eventually be connected to a switch for multi-channel slow sensing [35] [39], [40], in this architecture with EBF fibers the system is arranged into a network of N fibers, each used as a distributed sensor. Hence, the system is based on 3 blocks: OBR, distribution network, sensors.

The OBR, as reported in [21], [22], aims at resolving in the backreflections occurring at each fiber location by means of a swept-laser OFDR. In its minimal implementation, the system is divided into two branches: the sensing branch is a swept-laser interferometer based on a network of 50/50 splitters, and connected to the fiber sensors; the trigger branch is itself an interferometer, which uses a fiber delay line having the same length of the fiber under test [41], [42]. The output of the 2 interferometers is collected with a photodetector (PD) which is accurate enough to detect power values in the order of −110 dBm (10 fW), and then processed with a DAQ (data acquisition) for Fourier analysis [20], [22].

The key principle to turn the OBR into a sensing network is the use of scattering-level multiplexing (SLMux) [29], [30] [38], which can be considered as a

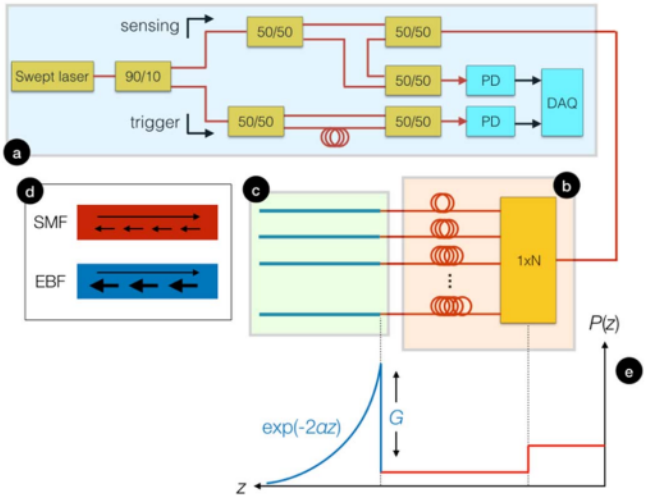

Fig. 1. Schematic and working principle of a OBR sensing network based on enhanced backscattering fibers. The system is composed by three building blocks: (a) OBR system, implemented as a swept wavelength interferometer; (b) distribution network, which implements splitting and individual channel delaying; (c) array of EBF fibers, implementing distributed sensors. (d) Sketch of a distributed sensor based on EBF with respect to a SMF. (e) Trace of the power P backreflected to the OBR for each location z: the initial power, attenuated through the splitter, is enhanced by the scattering gain factor (G) and attenuated with the exponential law of attenuation.

variation of spatial division multiplexing (SDM) [43]–[45]. In SDM, signals travels at the same time and bandwidth, and are spatially separated by exploiting the propagation properties of the fiber. Solutions have been proposed based on multi-core fibers [43], [44] or few-mode fibers [45], where the orthogonality is encoded in the fiber modes. In SDM-based sensors, however, the sensors are all within the same fiber [43], limiting the potential applicability of the method; these methods are mainly used in shape-sensing [46]. SLMux, likewise, encodes the multiplexing into spatial variations of the fiber propagation properties, in this case the Rayleigh backscattering; however, the diversity conditions comes from applying a different delay to each fiber such that each EBF contributions is located at a different spatial location [38]. We label this condition as the *scattering diversity*, and it is implemented by having a distribution network formed by different delay lines, each applying a different time-delay to individual channels. Sensors are then formed by EBF fibers, which have a backscattering level much larger than a standard fibers.

OBR SLMux networks are then characterized by a combination of standard single-mode fibers (SMF) and enhanced backscattering fibers (EBF); SMF works within the distribution network, while EBF represent the several distributed sensors.

In a single-channel, Fig. 1(e) shows the power trace, i.e. the power backreflected into the OBR at each location. The power backscattered by an EBF is significantly larger than a SMF; hence, at each EBF location the contributions of the other SMF fibers acts as a noise contribution, as shown in [28], [29]. This is shown in Fig. 2, where a 4-channel SLMux trace is shown; experimentally, up to 12 SLMux channels have been arranged by the authors, while we expect that system can work up to 64 channels [38], the maximum extent of commercially

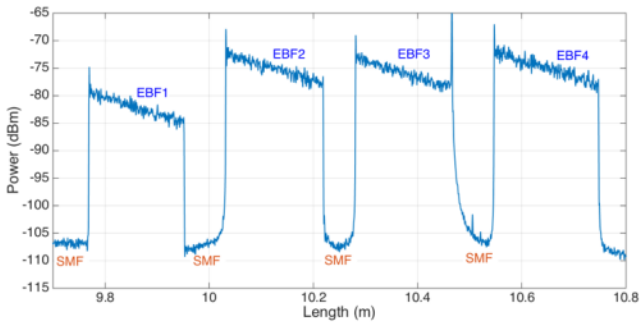

Fig. 2. Backscattering trace of a 4-channel SLMux network, implemented with 4 spans of 0.2 m EBF fibers.

available splitters. The EBF contributions are >30 dB higher than SMF scattering level, which implies that the distribution SMF fibers act as a mere delay line, but the scattering from the EBF is not significantly perturbed by the SMF contributions, and the OBR can detect and isolate each EBF sensing fiber.

III. Theory of Enhanced Backscattering OBR

The starting point for the analysis has been reported by Froggatt and Moore [21], which reported the propagation problem of the light wave field into a medium having elastic scattering [25]. For an optical fiber, as for any waveguide, the electric field $E(z)$, where z is the fiber location, obeys to the homogeneous wave equation (HWE) [47], adjusted for the scattering term:

$$\frac{\partial^2 E(z)}{\partial z^2} - \gamma^2 \left[1 + \frac{\Delta\varepsilon(z)}{\varepsilon}\right] E(z) = 0 \tag{1}$$

where γ is the complex propagation constant. The term $\Delta\varepsilon/\varepsilon$ contains the scattering phenomena occurring in the fiber, which account for the local reflections at each fiber location: ε is the dielectric permittivity of the fiber, while $\Delta\varepsilon(z)$ contributes to the local reflections that are both function of the wavelength and of the space [21].

The complex propagation constant is expressed as:

$$\gamma = \alpha + j\beta. \tag{2}$$

The real part α corresponds to the fiber one-way losses, while the imaginary part β is the wavenumber. While for a SMF fiber we can always assume that $\alpha \approx 0$ since the losses are truly negligible, for an EBF fiber losses are significant. According to [38] the two-way losses of EBF fibers in the infrared range from 30 to 300 dB/m, which means that for these fibers α ranges from 3.45 to 34.5 m^{-1}. On the other side, $\beta = 2\pi n_{eff}/\lambda = 5.9 \times 10^6$ rad/m for EBF fibers having $n_{eff} = 1.464$ operating in the infrared wavelengths around $\lambda = 1550$ nm. Hence, $\alpha \ll \beta$ and we can solve the equations considering $\gamma = j\beta$.

As known from electromagnetics theory [47], the solution of the HWE yields the linear combination of two counter-propagating waves: a forward wave E_+ propagating in the positive direction $+z$, and a backward wave E_- propagating in the negative direction $-z$. The scattering events yield an extremely small reflectivity, i.e. $\Delta\varepsilon/\varepsilon \ll 1$. This is true for SMF fibers, but also for EBF fibers: despite having scattering increments up to 50 dB over an SMF [38], the return loss of these fibers is still $< 10^{-5}$ which allows to both neglect standing waves existing between multiple sections of the fiber, and to consider the forward wave unaffected by the local changes of the reflected wave. Hence, we can write:

$$E(z) = E_+ e^{-j\beta z} + E_-(z)\, e^{j\beta z}. \tag{3}$$

Then, we can calculate the second order derivative of $E(z)$ with respect to z, and obtain the first term in Eq. (1):

$$\frac{\partial^2 E(z)}{\partial z^2} = -\beta^2 \left[E_+ e^{-j\beta z} + E_-(z)\, e^{j\beta z}\right] + 2j\beta \frac{\partial E_-(z)}{\partial z} e^{j\beta z} \tag{4}$$

where we apply the slow-rate approximation [21], [48]

$$\frac{\partial^2 E_-(z)}{\partial z^2} \approx 0. \tag{5}$$

The approximation in Eq. (5) is valid for all conditions in which the rate of change of the backreflected wave is not very large. In fact, it works well in either SMF or EBF fibers, but not during the SMF/EBF transitions where the backreflected power fluctuates well over 30 dB in few micrometers; however, these transition regions, well visible in Fig. 2 with a ripple artefact, are not interesting for sensing, but rather belong to the distribution network. Using this result, we can solve Eq. (1):

$$\frac{\partial^2 E_-(z)}{\partial z^2} = \frac{-j\beta}{2} \frac{\Delta\varepsilon(z)}{\varepsilon} \left[E_+ e^{-j2\beta z} + E_-(z)\right]. \tag{6}$$

Considering that $|E_+| \gg |E_-|$ due to the small amplitude of scattering events, we can neglect the second term in Eq. (6):

$$\frac{\partial E_-(z)}{\partial z} = \frac{-j\beta}{2} \frac{\Delta\varepsilon(z)}{\varepsilon} E_+ e^{-j2\beta z}. \tag{7}$$

Now, as shown in [21], [48], we can integrate the left and right term over z:

$$E_-(z) = \frac{-j\beta E_+}{2} \int_{-\infty}^{+\infty} \frac{\Delta\varepsilon(z)}{\varepsilon} e^{-j2\beta z} dz. \tag{8}$$

The left term of Eq. (8) is the backreflected wave, acquired on the OBR instrument with the swept-laser system of Fig. 1(a). The right term, aside from a constant, is the Fourier transform of the local permittivity change, which is the *signature* of the fiber under analysis, evaluated at twice the wavenumber of the input wave:

$$E_-(z) = \frac{-j\beta E_+}{2} F\left\{\frac{\Delta\varepsilon(z)}{\varepsilon}\right\}(2\beta). \tag{9}$$

Computationally, this is the same result that we observe from a standard fiber. The work from Froggatt and Moore [21] shows how evaluate the fiber signature from the backreflected wave at the same frequency, exploiting the properties of the Fourier transform. This process is performed by the OBR software.

The results of Eq. (1)-(9) have been obtained for OBR working with a single fiber. For a SLMux system with N channels as described in Fig. 1, the E_- wave is formed by

the sum of the N signatures $\Delta\varepsilon_i/\varepsilon$, where $i = 1, \ldots, N$ refers to the i-th channel.

Nevertheless, we can still solve the OBR system as in a single-fiber system, but imposing 2 assumptions. The first one is that, as shown in [38], [49], the i-th and k-th signatures behave almost as statistically independent random signals, since the scattering elements in each different fiber are unrelated. This assumption is valid for both SMF and EBF, and has been experimentally shown in [38], where the cross-correlation between different signatures have been shown to be very approximated with an additive white Gaussian process. The second assumption is the scattering diversity, which is the underlying SLMux principle: given that the i-th EBF fiber sensor has length L_i and is located within the lengths z_i (starting point) and $z_i + L_i$ (end point), no other k-th EBF fibers is located in the same location; in formula:

$$[z_i \div (z_i + L_i)] \notin [z_k \div (z_k + L_k)] \quad \forall i \neq k. \tag{10}$$

Hence, on each i-th fiber, we see the overlap of one and only one high-scattering fiber and (i-1) SMF fibers. The worst case scenario is for the shortest branch of the distribution network, which interferes with (N-1) other channels. Nevertheless, the OBR can be still resolved as in Eq. (9) *only on the EBF spans*, if we assume that:

$$E_{-,EBF}(z) \gg NE_{-,SMF}(z). \tag{11}$$

where EBF and SMF subscripts refer to each type of fiber, respectively. To verify the limit of this statement, we can consider the backscattered trace $P_i(z)$ which is the power detected on the OBR at each location. Since we are resolving the system only on the $z_i \div (z_i + L_i)$ intervals, the power follows the attenuation law [47]:

$$P_i(z) = GP_{SMF}e^{-2\alpha(z-z_i)}. \tag{12}$$

The parameter G defines the *scattering gain*, which is defined as the ratio between the power scattered by the EBF and the power P_{SMF} backscattered by a SMF [29]. Results in [26-37] show that the scattering gain of EBF can be 30-55 dB, hence very significant although well within the limits of OBR theory. The term 2α refers to the fiber losses, accounted both forward and backward since the fiber is reciprocal.

Since one EBF fiber interferes with (N-1) SMF signatures in the worst case, all statistically independent on each other, we define the signal-to-interference ratio (SIR) as the ratio between the $P_1(z)$ and (N-1) times P_{SMF}, assuming that the channel 1 is the shortest in the distribution network:

$$SIR(z) = \frac{Ge^{-2\alpha(z-z_1)}}{N-1}. \tag{13}$$

By imposing the minimum SIR required to work in the system, we can finally evaluate the maximum length of each EBF sensor L_{max}:

$$L_{max} = \frac{1}{2\alpha} ln\left[\frac{G}{SIR(N-1)}\right] \tag{14}$$

which is in accordance with [30]. This result can be empirically verified in Fig. 2, where we observe that despite the high losses of the EBF, at the end of each sensing length the backscattered power is still >30 dB higher than the combination of all SMF values. Eq. (14) provides an estimate of the maximum length of a SLMux network given the fiber parameters G and 2α and the number of channels.

The level of SIR required for successful operation depends on the method used to resolve the scattering signatures; OFDR/OBR methods that resolve by correlation in the frequency domain [19]–[22] can operate even with low SIR levels since the correlation operator is noise-resilient and the overlapping signatures are statistically independent [38]. On the other side, methods that operate directly on the backscattered power require higher values of SIR to operate [26], [27]. In any circumstance, the losses of the system, including the $1\times N$ splitter, do not affect the SIR since they apply to both the SMF and EBF fibers; instead, the SIR is affected by the channel imbalances, e.g. channel-dependent loss of the splitter and local variations of the EBF attenuations.

IV. Fabrication and Characterization of Enhanced Backscattering Fibers

The results presented so far are valid for any swept-wavelength OBR working in the near infrared. The experimental characterization of the fibers has been carried out using a commercial OBR4600 (Luna Inc., Roanoke, VA, US) interrogation system, with 88 nm laser sweep bandwidth and 10 μm spatial resolution.

A. Methods for Scattering Enhancement

As seen from Eq. (14), OBR networks that implement simultaneous detection require high values of G while maintaining low losses in order to operate over significant lengths, since the lengths that can be interrogated grow with ln(G) but decreases linearly with α.

We can identify two approaches for achieving a high reflectivity: design a fiber that is inherently high-scattering and can be interfaced with a SMF; or manipulate a SMF or similar fiber in order to locally increase its reflectivity. Table I reports the performance achieved by each method.

The first approach relies on fabricating fibers having tailored Rayleigh scattering and absorption, and the main method that has been proposed is the use of nanoparticle-doped fibers [50]–[54]. Dielectric oxide nanoparticles (NP) are known to have very high elastic scattering, which makes it a good candidate for EBF. Fibers doped with nanoparticles have been reported in [50]–[52], and have mainly been used for the design of random amplifiers and fiber lasers [55], without however exceeding the performance and efficiency of modern Er/Yb-doped fibers [56]. But thanks to the advent of OBR, NP-doped fibers have now become a new technology of interest.

Among this class of fibers, the most successful results have been achieved through the use of MgO-based nanoparticle-doped fibers (MgO-NP) [50]–[52], since the method of fabrication of this fibers is simple, and fibers can be design to match the sizes of SMF fibers.

The process of MgO-NP fabrication has been described in [52]. The fiber, originally designed as a 1550-nm amplifier,

TABLE I
COMPARISON OF SCATTERING-ENHANCEMENT METHODS AND THEIR PERFORMANCES FOR OBR SENSING

Reference	Method	G (dB)	2α (dB/m)
[26]	MgO-NP fiber, NP ring	47.5	298
[27]	MgO-NP fiber, NP ring	46.1	292
[28-29]	MgO-NP fiber, inner-core	45.2	33.1
[30]	MgO-NP fiber, inner-core	36.5	25.5
[31]	MgO-NP fiber, inner-core	32.3	27.8
[32]	Direct FBG inscription on MgO-NP fiber	37.2+28.0 (FBG)	22.1
[33]	fs-laser inscription of 25 cm mini-grating on SMF	40-45	15-40
[34]	High-NA high-Ge-doped fiber	10	Not inferred
[34]	UV-exposure of SMF fiber	20	Not inferred
[35-36]	UV-exposure of H_2-loaded SMF fiber	37	Not inferred
[36]	Ge/B doped Redfern fiber	10	Not inferred
[37]	Random optical grating by UV exposure	30	Not inferred

has size matching the SMF-28 telecom fiber (10/125/250 μm core/cladding/jacket diameter). The first step is the fabrication of the preform, which is performed using MCVD (modified chemical vapor deposition); the preform is made of silica glass, and the core is doped with a solution of $MgCl_2$ and $ErCl_3$, which contributes for an additional scattering increase. The final step is fiber drawing, which is performed in a standard draw-tower; during the MCVD process, due to the high temperature, the separation of silica and alkaline-earth ions produces a compound rich of MgO spherical particles, which are elongated in the fiber; the particles have diameter from few nm up to hundreds of nm [51], [52]. MgO-based nanoparticles within the silica fiber are the main contributors to the Rayleigh scattering enhancement, and they do have scattering signatures very similar to SMF [38]. MgO-NP fibers have been reported in [26]–[32], using two different type of designs. In [26-27], MgO-based nanoparticles have been deposited in a ring around the fiber core, while in [28]–[31] nanoparticles are distributed all around the core. The ring configuration achieves gain over 46 dB (40,000 times a SMF), but the penalties are high two-way losses, approaching 300 dB/m. The second configuration, in which the inner part of the core is doped with MgO-based NP, achieves a gain of 32-45 dB, but losses are an order of magnitude smaller (22-33 dB/m). MgO-NP fibers perform much better than Ge-doped [34] and Ge/B-doped [36] fibers, in which G is limited to $\sim$10 dB.

The second EBF approach starts from SMF fibers, and locally increases the reflectivity. A possible solution is the exposure of the fiber to UV (ultraviolet) light. The solution proposed by Loranger *et al.* using a setup originally designed for fiber Bragg grating (FBG) inscription, and documented in [34], makes use of a 213 nm laser source exposing the fiber for 4 seconds per each 50 μm fiber length (spot size of the laser). The setup uses a motion controller for exposing a long fiber length to continuous UV light. This arrangement allows achieving a gain of 20 dB [34] to 37 dB [36], depending on whether the SMF fiber is hydrogen-loaded in a pressurized chamber, and the losses are undisclosed and appear to be low.

The alternative solution is to inscribe a grating reflector in the fiber; although this method is not formally equivalent to Rayleigh scattering, since the grating provides a continuous backreflection that is not a scattering event, direct inscription of random structures into SMF fibers yields a result that is very similar from the OBR point of view. Yan *et al.* reported a method based on femtosecond laser inscription of a narrow grating over 25 cm of SMF [33], achieving similar results to MgO-NP (40-45 dB gain, 15-40 dB/m losses). The setup used in this approach is derived from the inscription of long regenerated gratings [57]. Along this line, Monet *et al.* have recently reported a random optical grating inscribed with a UV laser, that achieves a 30 dB reflectivity enhancement over 8 nm bandwidth, suitable for OBR-based sensing. In [37], an FBG over a MgO-NP fiber was demonstrated, raising the reflectivity level by an additional 28 dB. As a key distinction, while the inscription of long weak FBGs is based on a periodical refractive index modulation [19], [33], [32], [57], a random-grating approach scrambles the periodicity of the refractive index which result in a wide increase of the reflective bandwidth [37], [58].

In terms of sensing network design, the two approaches have different characteristics. MgO-NP fibers is today a well-consolidated technology, and they are handled as a standard fiber: MgO-NP fibers can be drawn spooled like all commercial fibers in kilometers per each preform, they can be stripped, cleaved, and spliced as a standard SMF fiber using the SMF-SMF splicing modes with minimal losses (<0.1 dB), and the fiber used in sensors maintains its original protective jacket which is essential in medical devices. Most importantly, the fabrication is suitable for a standard drawing tower for telecom fibers. The main drawback is the need for a distribution network that requires splicing several SMF fibers with different length (from the splitter lead to each EBF), but this can be potentially circumvented using programmable delay lines [42]. On the other side, gratings and UV exposure have the advantage that the user can expose any part of the fiber, arbitrarily, simplifying the distribution network. There are however 2 main drawbacks: at first, the process of inscription is very slow (0.1 to 2 mm/s in Yan *et al.*'s work [33]), which complicates the design of large sensing networks. In addition, both grating inscription and UV exposure processes require stripping the fiber jacket, which significantly reduces the fiber tensile strength, limiting the application.

B. Characterization of Sensing Properties of MgO-NP

The key optical parameters of MgO-NP that affect the sensing performances are: (1) profile of the mode transmitted into the fiber; (2) sensitivity to strain/temperature; (3) sensitivity to the surrounding refractive index as a function of fiber thickness.

The profile of the LP_{01} mode transmitted though the fiber allows evaluating the mode confinement, and whether the NP shape and distribution affects the properties of the light through the structure. As in [26], [31], we simulated the shape of the LP01 mode, simulated with COMSOL

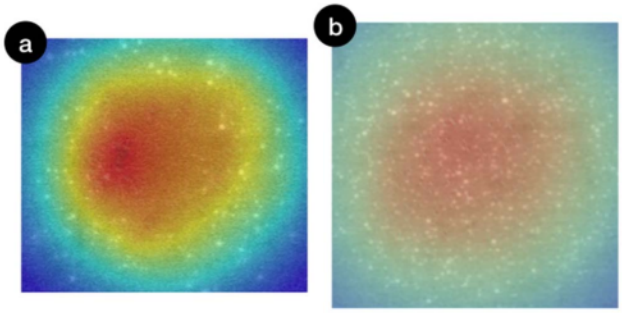

Fig. 3. Profile of the LP_{01} mode propagating in the MgO-NP fiber configuration. The chart shows the scanning electron microscopy (SEM) view of the NP-doped core (the width of the pictures corresponds to 10 μm) in the background, and in transparency the estimated field intensity of the light by means of 2D-grid simulation. (a) Fiber with MgO-based nanoparticle arranged in a ring around the core [26]; (b) Fiber with MgO-based nanoparticles located in the core [30].

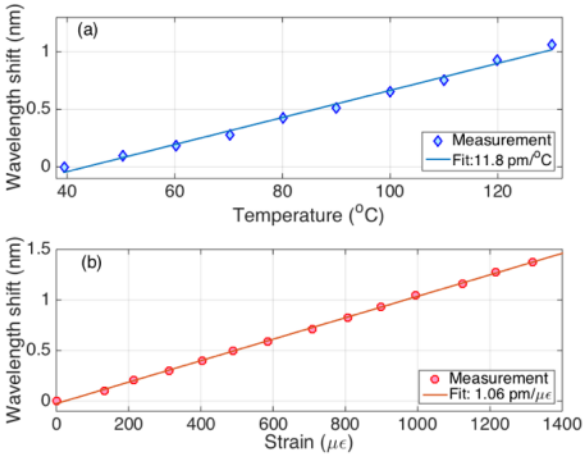

Fig. 4. Sensitivity evaluation of a MgO-NP fiber to (a) temperature and (b) strain. Data have been acquired by recording the wavelength shift from the reference condition for each temperature/strain value.

Multiphysics (Comsol Inc., Burlington, US), for ring-based nanoparticles [26]–[27] and for inner-core nanoparticles [28]–[31]. The result is shown in Fig. 3, where the transparency in background shows the SEM (scanning electron microscopy) view of the core cross-section. Overall, the mode has a shape similar to the SMF LP_{01} mode, which implies that the SMF-EBF mode conversion is efficient. The results in Fig. 3 suggest that the effect of nanoparticles, which is evident in the scattering gain, has a minimal effect onto the fiber propagation, and therefore we can treat the EBF as a standard fiber on the OBR interrogation.

In Fig. 4 we report the temperature and strain sensitivity of the MgO-NP EBF, which are defined as the wavelength shift, recorded in each section of the fiber, per each unit of temperature or strain change. The chart, obtained through an experimental calibration, shows that the sensitivity of the fiber is linear, and similar to a standard SMF. The thermal coefficient is 11.8 pm/°C, while the strain coefficient is 1.06 pm/$\mu\varepsilon$. These values are similar to the nominal sensitivity of glass fibers (10 pm/°C, 1 pm/$\mu\varepsilon$ [59]), since they depend on the fiber compound, which is made of silica; the effect of nanoparticles

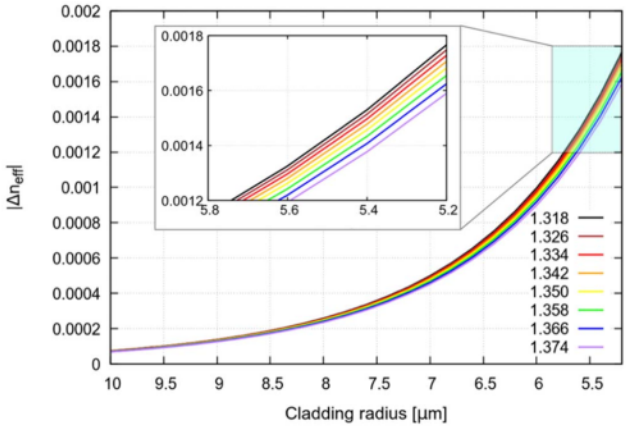

Fig. 5. Change of the effective refractive index Δn_{eff} of the MgO-NP fiber n_{eff} as a function of the change of the radius of the fiber cladding, for different values of refractive index; the inset shows the thin fiber portion.

TABLE II
OBR SETTINGS FOR DISTRIBUTED SLMUX SENSING

Parameter	Settings
Wavelength scan range	1525 – 1610 nm
Measurement frequency	3 Hz
Group index of the fiber	1.464
Sensor spacing	0.101 cm
Gage length	0.249 cm
Electrical amplification	None
Sensing range	8 to 120 cm
Wavelength shift calculation	Normalized cross-correlation
Digital filtering	Butterworth low-pass 5th order

on the sensitivity is negligible (NP volume fraction is about few %). Results have been obtained by calibrating a single MgO-NP fiber in a single point, but they are well repeatable throughout the MgO-NP fibers used in experiments [28]–[32].

The possibility of detecting refractive index changes with a MgO-NP fiber has been explored in [26], [31]. In this case, the cladding thickness has to be thinned, through wet etching. When the fiber cladding gets thinner, the fiber becomes sensitive to the surrounding refractive index (RI), as shown in the simulations of Fig. 5. When the cladding radius gets thinner, moving onto the right part of the chart, we observe a change of the fiber n_{eff}, similar to the change experienced by strain or temperature change. The sensitivity increases exponentially with the fiber thickness reduction, and as seen in the inset, for a defined thickness we experience a variation Δn_{eff}, of the effective fiber refractive index, which allows the measurement of RI.

With these parameters, we have implemented distributed sensing using the OBR settings listed in Table II.

V. APPLICATIONS OF ENHANCED BACKSCATTERING OBR SENSING NETWORKS

The SLMux-based distributed sensing networks based on EBF fibers have found several applications, mainly in biomedical engineering where there is a strong need to fit numerous fibers in a small volume for multi-dimensional sensing [8].

Emerging applications also show the EBF properties in harsh environments [60].

A. Multidimensional Temperature Sensing in Thermotherapies

The *in situ* measurement of temperature with minimally invasive devices plays a significant role in modern thermotherapies [8], as thermometry is the physical driver behind surgical operations. The main application of SLMux networks has been reported for minimally invasive thermal ablation of tumors [61]–[63]. Several thermal ablation methods have been reported, using radiofrequency, microwave, laser, or high-intensity focused ultrasound sources [63]; the common factor of these processes is to deliver electromagnetic energy from a miniature applicator to the surrounding tumor, in order to heat the cells over their mortality rate [64], [65]. In such fashion, thermal ablation is a rapid percutaneous procedure, which usually requires local anesthesia [62].

Thermal dosimetry models suggest that the cytotoxicity levels of cancer cells starts at 42-44 °C [64], while the protein coagulation occurs, almost instantaneously, around 60 °C [65]. In order to correctly estimate the amount of tissue ablated in real time, and therefore ensuring that the thermal dose is sufficient to treat the volume of the whole tumor, fiber optic sensors [8], [61] and imaging [66], [67] have been used. Here, the key and unprecedented advantage of SLMux network is that they can interrogate multiple distributed sensors at the same time, hence they are prone to perform 2D or even 3D sensing with narrow spatial resolution. The fiber can operate *in* situ thanks to its biocompatibility, in accordance to ISO 10993 standard concerning the biological evaluation of medical devices [68]. Alternative methods, such as one-fiber OBR arrange on a plate [7], are usable only as a laboratory tool, but EBF fibers enable to bring this technology, potentially, *in vivo*.

The first SLMux work recording 2D temperature patterns have been reported in [28], using 4 MgO-NP fibers to detect the temperature during an *ex vivo* radiofrequency ablation of a liver. The fibers have been arranged on a $x \times y$ grid of 2.5 mm × 5.0 mm step (x = spatial resolution of OBR; y = distance between adjacent fibers), with size 40 mm × 15 mm; hence, the 68 sensing points are laid on a grid with pixel size 12.5 mm^2. Upon reconstructing the temperature data, the authors obtained a 2D thermal map in real time; a sketch of the thermal map, at 5 seconds interval, is shown in Fig. 6. The results obtained with 2D sensing have been recently reported also for laser ablation of tissues, with a similar 4-fiber architecture [69], [70].

This result has been extended to 3D sensing, using a highly dense SLMux configuration with 12 fibers, as shown in Fig. 7 and reported in [71], to record thermal maps during microwave ablation of liver tissue. The *xyz* grid has been arranged by displaying 8 fibers along a 16 mm grid, and 4 fibers at the vertices of a 8 mm square around the applicator, located at the origin of the axes. The spatial resolution along y is 2.5 mm. Data reported in Fig. 7 show the inner part of the overall volume of 10,240 mm^3, on which 204 sensing points have been located, for an average voxel size of 50.2 mm^3, which is a result comparable

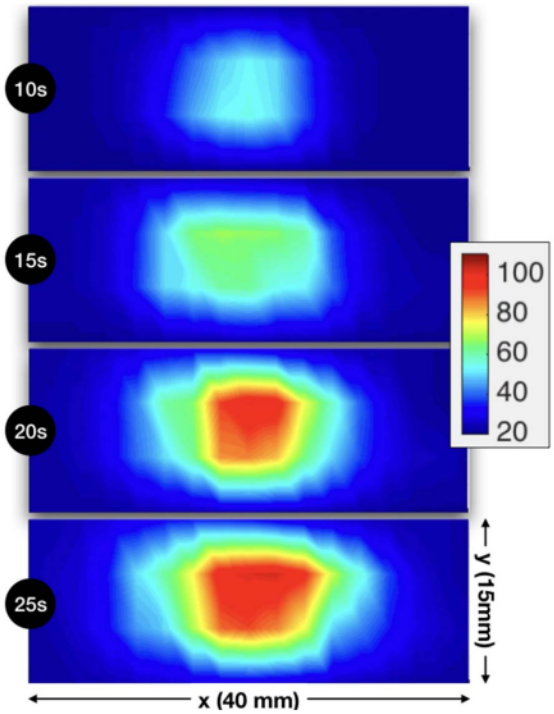

Fig. 6. 2D thermal map acquired with a 4-channel SLMux [28]; the chart shows the temperature on the *xy* grid after 10 s, 15 s, 20 s, 25 s elapsed time. The shape of the ablated region can be inferred from the 60 °C isothermal contour. The color bar shows temperature in °C.

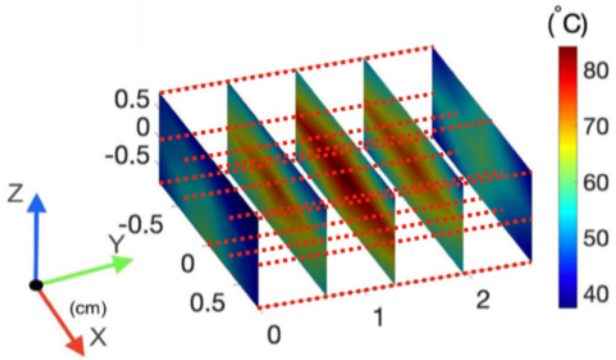

Fig. 7. 3D thermal map acquired with a 12-channel SLMux; the chart shows the temperature in a 3D space, with 12 fibers laying on the *xz* plane along *y* axis.

with magnetic resonance imaging [66], [67]; SLMux however has significant advantages in terms of accuracy, cost, and stability due to respiratory rate of patients [61]. The data in Fig. 7 show the potential of 3D sensing: thermal maps have been sliced in a plane-by-plane view (for the sake of visualization, only 5 planes are shown), and allow an estimation of the heat delivery in each radial direction with a method that is faster (0.3 Hz vs 2 Hz) and more accurate (±0.4 °C vs 2 °C) than MRI (magnetic resonance imaging) [67].

Overall, *in vivo* thermal sensing is a significant application for OBR densely multiplexed network, as it allows the real-time detection of the ablated tissue and isothermal regions in real time, providing clinicians with a tool to increase the clinical efficacy through advanced thermometry.

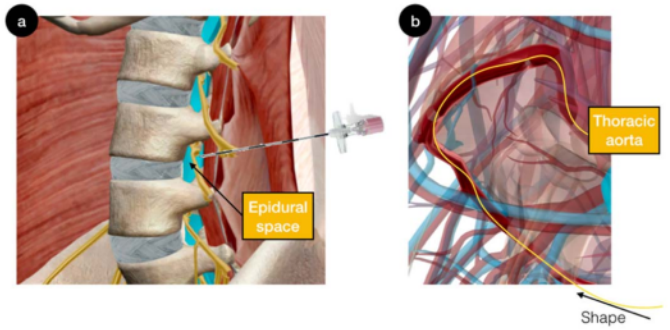

Fig. 8. Anatomic sketch of shape-sensing OBR sensing network applications. (a) Epidural anesthesia scenario [28], where a Tuohy needle is percutaneously inserted through the epidural space behind the *ligamenta flava* (highlighted), within L03 and L04 vertebrae. (b) Shape-sensing of cardiovascular devices [35], where a flexible device is inserted in proximity of the thoracic aorta, complementing imaging techniques.

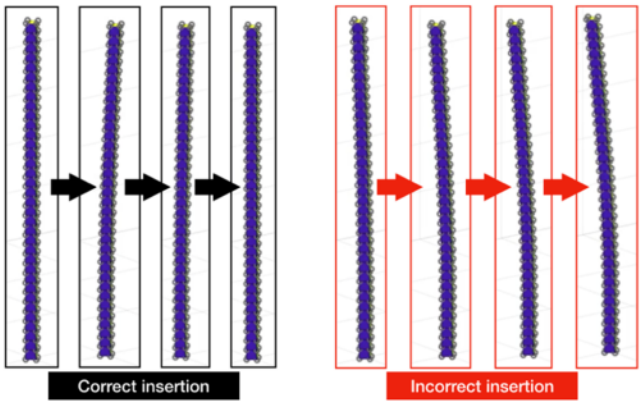

Fig. 9. Bending estimation in epidural anesthesia shape sensing [28]; left: correct insertion; right: incorrect insertion. Each marker shows the location of a sensing point along the needle.

B. Strain and Shape Sensing of Medical Devices

Exploiting the potential of multi-dimensional strain sensing, OBR networks have been applied to shape sensing of surgical devices. Two main applications have been recently demonstrated, and sketched in Fig. 8, exploiting the multi-fiber EBF sensing.

In the first one, reported in [28] and sketched in Fig. 8(a), the shape sensing technology is applied to the narrow bending of a rigid metallic percutaneous needle. The application proposed by Beisenova *et al.* [28], [72] aims at providing a clinical guidance for epidural anesthesia [73]–[77]. During an epidural insertion, a Tuohy metallic needle (8 cm length, 1.32 mm outer diameter, 90° bending on the tip) is inserted by a clinician piercing the skin, through a layer of tissues (subcutaneous fat, supraspinous and interspinous ligaments) to reach the epidural space behind the *ligamentum flavum* located within the L03 and L04 vertebrae, and highlighted in Fig. 8(a). The sequence of layers having different stiffness impresses specific bending patterns to the needle, according to [77]; a correct insertion of the needle reaches a soft zone in correspondence of the epidural space, after crossing a stiff tissue; an incorrect insertion causes about twice as much bending in proximity of the tip [75].

Solutions for epidural space identification has been proposed based on qualitative parameters such as the drop of resistance of the needle through the insertion [75]. Recently, FBG-based optical sensors have been proposed, to detect the change of pressure at the needle tip [73], [74]. The main drawback of these techniques is that they can discriminate whether the probe has reached the epidural space, but do not help guiding the clinician to the target; this, according to Arendt and Segal [76], is one of the failure causes of epidural anesthesia.

The solution proposed by Beisenova *et al.* [28] makes use of a quadruplet of fibers, mounted at the 4 cardinal points on the outside of the needle. This solution allows computing the directional strains along the direction of bending (east/west, north/south) and the common-mode strain which resolves the temperature compensation. By using a trigonometrical model suitable for low curvatures, a 3D reconstruction of the needle shape has been achieved. In the experiments, correct insertions were characterized by bending angle $<1.5°$, while incorrect insertions caused bending $>2.5°$ in the inner needle section. Fig. 9 shows the sequence of bending patterns provided in [28]: in a correct insertion, the needle bends and then straightens up as it crosses the softer layers; in an incorrect insertion, the needle progressively increases bending, moving onto the opposite direction. This elegant solution serves as a true guidance, because it renders position, shape, and correctness of the insertion in real time [28], [29], [72], and sensors mounted externally to the needle do not affect the inner fluid delivery.

Multi-fiber shape sensing, with 3 fibers, has been exploited also by Parent *et al.*, and reported both for the monitoring of a radiofrequency ablation multi-tip device [36] and, more recently, as a guidance system for cardiovascular medical devices [35]. This latter configuration is sketched in Fig. 8(b).

The shape-sensing method proposed in [35] addresses the problem of trans-arterial guidance or a chemo-immobilization device. The sensing head is formed by a fiber tripled, each fiber at the vertices of an equilateral triangle in order to convert the 3D forces into curvature, mounted on a 5-Fr (1.67 mm diameter) device. The method uses OBR, with curvature identification, in conjunction with a MRI angiography and arterial tree segmentation, to form a guidance system for the positioning and navigation of the medical device to the point of treatment. This solution, which uses EBF in lieu of standard SMF fibers [78], provides an improvement of shape detection accuracy [36].

C. Refractive Index Detection

The possibility of using the EBF fibers for RI sensing is a recent development, reported in [31] for a single-fiber system and in [26] in multi-fiber, SLMux configuration. RI optical fiber sensors, or optical fiber refractometers, are an important tool for chemical and biological sensors, and find applications in biology, diagnostics, food processing, agriculture and aquaculture, and environmental sciences [79].

RI sensors are usually based on a reflection or transmission device inscribed in the fiber [80]–[85]: the most popular technologies make use of a Bragg grating [80], [81],

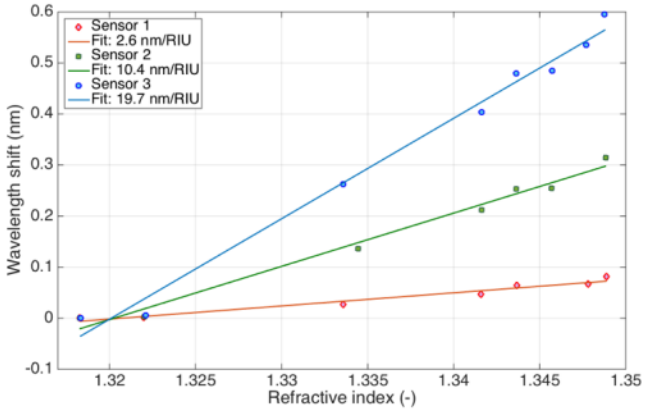

Fig. 10. Sensitivity of 3 etched MgO-NP sensors to RI changes.

an interferometer [82], or a surface plasmon resonance device [83]–[85]. Recently, distributed RI sensors methods have been proposed [4], [13] making use of in-line fiber multiplexing.

In [31], Sypabekova *et al.* proposed for the first time the design of a RI sensor based on an etched MgO-NP. Etching the fiber, with a 48% solution of hydrofluoric acid, is an industrially scalable process, similar for example to the etching of photoresist layers in electronic circuits; hence, a RI sensor based only on an etched fiber would be significantly easier to fabricate. The principle of operation is that, when the cladding of the fiber is progressively etched away, we observe a change of n_{eff}, which results in a wavelength shift. This is the same principle of etched FBG sensors [80], but rather than encoding the n_{eff} change into a notch-band FBG spectrum, it is encoded into the Rayleigh scatter signature [21]. However, by etching the fiber, we significantly reduce the confinement factor of the electric field, introducing significant losses which become higher as the sensitivity rises. An etched SMF would not have enough reflectivity to sustain the additional losses due to the lower confinement factor, which as shown in [26] are as high as 30 dB (and account for up to 4.2 dB/mm in the etched portion). On the other side, a MgO-NP fiber has enough scattering intensity to sustain etching losses and still detect a wavelength shift.

In this sense, the etched MgO-NP sensor can work in two ways, depending on the domain of interrogation. In the pivotal work presented by Sypabekova *et al.* [31], the etched MgO-NP fiber has been interrogated in the wavelength (frequency) domain, measuring the spectral shift of the Rayleigh spectral signature, in a similar fashion to most biosensors. The sensitivity obtained with this method depends on the thickness of the fiber, as shown in Fig. 5. Given that the fiber is etched along a portion, the sensor exhibits a sensitivity over multiple points; it is possible then to interrogate the wavelength shift in the most sensitive points.

In Fig. 10, we show the RI response of 3 different sensors fabricated with etched MgO-NP EBF fibers. The sensitivity of the probes ranges from 2.6 nm/RIU (refractive index units) for the shallow-etched sensor to 19.7 nm/RIU for the deep-etched version of the probe.

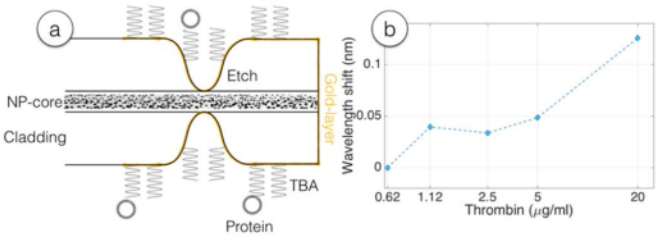

Fig. 11. Prototype of a thrombin reflector-less biosensor. (a) Design of the probe; (b) Wavelength shift as a function of thrombin concentration.

As for temperature or strain sensors, given that the MgO-NP sensors raise the scattering levels with a significant SIR, Ayupova *et al.* [26] showed the possibility to multiplex RI sensors into a SLMux network, for detection of a plurality of RI and temperature sensors.

The second method of interrogation is in time domain, according to the work presented by Korganbayev *et al.* [27]. The key principle is to convert the change of n_{eff}, into a time delay, and correlate the fiber traces obtained at different RI values. The sensitivity obtained with this method has been reported as 9.69 ps/RIU, which corresponds to a length change of 5.25 mm per each RIU change. This method, albeit innovative, does not allow distributed sensing, but it can be potentially be extended to simpler OFDR systems.

D. Reflector-Less Biosensors

RI sensors are the building block of biosensors, through a functionalization step that makes the probe sensitive to the specific analyte under investigation. The functionalization of a MgO-NP EBF to protein sensing has been described in [86]. This architecture is labeled as a *reflector-less* biosensor: compared to sensors based on gratings, interferometers, or surface plasmonics, in this architecture there is no reflective (or transmission) element specifically inscribed in the fiber, but the sensing information is entirely encoded in the Rayleigh signature of the EBF, which is already a feature of the fiber itself.

The work reported in [86] constitutes the first prototype of MgO-NP fibers to protein biosensing and the main results are listed in Fig. 11. The functionalization has been carried out in a similar way to [87]: the etched fiber has been gold-coated with a 50-nm thin film, and thrombin-binding aptameters (TBA) have been deposited on the surface of the sensor for detection of thrombin, an important biomarker for cardiovascular diseases and thrombotic risks [87].

The result in Fig. 11(b) show the wavelengths shift measured for growing protein concentration from 0.62 to 20 μg/ml [87].

The possibility of designing reflector-less biosensors is a significant step in terms of easiness and scalability of device fabrication. Although the sensitivity is orders of magnitude below the thousands of nm/RIU recorded for many plasmonic devices or interferometers [79], the concept is the most minimalistic version of a fiber-optic biosensor with robust interrogation in the wavelength domain.

E. High-Temperature Sensing

The work reported by Yan *et al.* [33] extends the EBF applications to high-temperature sensing, exploiting the excellent thermal stability of the grating-based defects inscribed into the fiber to temperature values up to 800 °C. The micro-gratings, directly written in the fiber with a fs laser, show two key characteristics: no significant temperature-dependent loss, from room temperature to 800 °C; and a continuously linear sensitivity, equal to 11.9 pm/°C (0-250 °C) and 15.2 pm/°C (>250 °C). Although a spectral shift quality decrease was observed, the cross-correlation calculation is still reliable even at high temperature.

This work demonstrates the application of EBF in solid oxide fuel cells temperature detection. The temperature control of this type of cells allows an increase of efficiency and lifetime span, as the quality of energy generation is directly influenced by thermal stresses in the different locations of the cell. This result is significant, as it demonstrates that the EBF-based approach is more resilient to high-temperature sensing with linear sensitivity than bare SMF fibers.

F. X-Ray Radiation Sensing

The detection of radiation with optical fibers is an important sensing challenge, since fibers are suitable for operations in harsh radiation-prone environments [60]. The detection of radiation dosimetry in nuclear environment is concerned with the detection of high variable doses (thousands of Gy) [88]–[90], while medical applications require the detection of small constant dose levels (few Gy units) [91]. The only multiplexed radiation dosimetry works presented so far make use of FBG sensors, which show a low radiation sensitivity [88], [89].

The recent work from Olivero *et al.* [92] proposes the use of MgO-NP fibers for radiation sensing, using OBR interrogation. The principle of operation is the effective refractive index change as the fibers are exposed to radiation [90], which causes a wavelength shift of the spectral signatures. In this work, the authors observed a variation up to 72 pm, for a dose of 700 Gy/min over 10 minutes, with a linear increase of about 7.1 pm/min; this sensitivity value is about 5-fold increase over a bare SMF [88]. Data were observed with 5 mm spatial resolution, hence making the detection distributed.

VI. Conclusions

In conclusion, this work presents a tutorial on multi-fiber EBF-based distributed sensing networks, and reviews the present applications reported so far. The key innovation behind this development is the possibility of customizing Rayleigh scattering in optical fibers. For decades, the need to reduce losses in long-haul telecom systems has pushed to minimize Rayleigh scattering, down to its theoretical minimum. The recent advent of OBR, instead, calls for reversing the trend: increasing the Rayleigh scattering means augmenting the signal at the OBR detector. Several of the proposed method augments Rayleigh scattering from 3 to 5 orders of magnitude, but it is expected that future developments can find a better trade-off between scattering gain and fiber losses, as well as controlling the polarization as an additional factor.

Reconsidering the use of nanoparticles in optical fibers is a key asset, because this solution allows tailoring scattering properties while having a fiber that can be spooled, spliced, and easily interfaced. We envision that future OBR systems might include the distribution network within the system.

Multiplexing is the key of addressing the most advanced applications, and SLMux enables a new, high-density, multiplexing domain out of the scattering diversity. The main result is that we can now extend the OBR to a multi-fiber system. Distributed 2D/3D temperature sensing, as well as 3D-shape sensing, are inherently methods that require stacking multiple fibers in a miniature device, and SLMux-based OBR can now address these advanced applications. In addition, the possibility of designing reflector-less biosensors is also appealing, as it allows a facile fabrication of a fiber optic biosensor without any grating or interferometer.

References

[1] X. Bao and L. Chen, "Recent progress in distributed fiber optic sensor," *Sensors*, vol. 12, no. 7, pp. 8601–8639, 2012.

[2] C.-Y. Hong, Y.-F. Zhang, G.-W. Li, M.-X. Zhang, and Z.-X. Liu, "Recent progress of using Brillouin distributed fiber optic sensors for geotechnical health monitoring," *Sens. Actuators A, Phys.*, vol. 258, pp. 131–145, May 2017.

[3] X. Liu, B. Jin, Q. Bai, Y. Wang, D. Wang, and Y. Wang, "Distributed fiber-optic sensors for vibration detection," *Sensors*, vol. 16, no. 8, p. 1164, Jul. 2016.

[4] X. Lu, P. J. Thomas, and J. O. Hellevang, "A review of methods for fibre-optic distributed chemical sensing," *Sensors*, vol. 19, no. 13, p. 2876, Jun. 2019.

[5] A. L. Ricchiuti, D. Barrera, S. Sales, L. Thevenaz, and J. Capmany, "Long weak FBG sensor interrogation using microwave photonics filtering technique," *IEEE Photon. Technol. Lett.*, vol. 26, no. 20, pp. 2039–2042, Oct. 15, 2014.

[6] B. J. Soller, D. K. Gifford, M. S. Wolfe, and M. E. Froggatt, "High resolution optical frequency domain reflectometry for characterization of components and assemblies," *Opt. Express*, vol. 13, no. 2, pp. 666–674, 2005.

[7] E. G. Macchi *et al.*, "Optical fiber sensors-based temperature distribution measurement inex vivoradiofrequency ablation with submillimeter resolution," *J. Biomed. Opt.*, vol. 19, no. 11, Nov. 2014, Art. no. 117004.

[8] D. Tosi, E. Schena, C. Molardi, and S. Korganbayev, "Fiber optic sensors for sub-centimeter spatially resolved measurements: Review and biomedical applications," *Opt. Fiber Technol.*, vol. 43, pp. 6–19, Jul. 2018.

[9] A. Masoudi, M. Belal, and T. P. Newson, "A distributed optical fibre dynamic strain sensor based on phase-OTDR," *Meas. Sci. Technol.*, vol. 24, no. 8, Aug. 2013, Art. no. 085204.

[10] N. M. P. Pinto, O. Frazão, J. M. Baptista, and J. L. Santos, "Quasi-distributed displacement sensor for structural monitoring using a commercial OTDR," *Opt. Lasers Eng.*, vol. 44, no. 8, pp. 771–778, Aug. 2006.

[11] Z. Zhao, M. A. Soto, M. Tang, and L. Thévenaz, "Distributed shape sensing using Brillouin scattering in multi-core fibers," *Opt. Express*, vol. 24, no. 22, pp. 25211–25223, 2016.

[12] P. S. Westbrook *et al.*, "Continuous multicore optical fiber grating arrays for distributed sensing applications," *J. Lightw. Technol.*, vol. 35, no. 6, pp. 1248–1252, Mar. 15, 2017.

[13] P. J. Thomas and J. O. Hellevang, "A high response polyimide fiber optic sensor for distributed humidity measurements," *Sens. Actuators B, Chem.*, vol. 270, pp. 417–423, Oct. 2018.

[14] D. Chen, Q. Liu, X. Fan, and Z. He, "Distributed fiber-optic acoustic sensor with enhanced response bandwidth and high Signal-to-Noise ratio," *J. Lightw. Technol.*, vol. 35, no. 10, pp. 2037–2043, May 15, 2017.

[15] C. Wang *et al.*, "Distributed acoustic sensor using broadband weak FBG array for large temperature tolerance," *IEEE Sensors J.*, vol. 18, no. 7, pp. 2796–2800, Apr. 2018.

[16] M. Bravo, J. M. Baptista, J. L. Santos, M. Lopez-Amo, and O. Frazão, "Ultralong 250 km remote sensor system based on a fiber loop mirror interrogated by an optical time-domain reflectometer," *Opt. Lett.*, vol. 36, no. 20, pp. 4059–4061, 2011.

[17] M. A. Soto *et al.*, "Distributed temperature sensor system based on Raman scattering using correlation-codes," *Electron. Lett.*, vol. 43, no. 16, pp. 862–864, Aug. 2007.

[18] F. Peng *et al.*, "Ultra-long high-sensitivity Φ-OTDR for high spatial resolution intrusion detection of pipelines," *Opt. Express*, vol. 22, no. 11, pp. 13804–13810.

[19] J. Clement, G. Torregrosa, J. Hervas, D. Barrera, S. Sales, and C. R. Fernandez-Pousa, "Interrogation of a sensor array of identical weak FBGs using dispersive incoherent OFDR," *IEEE Photon. Technol. Lett.*, vol. 28, no. 10, pp. 1154–1156, May 15, 2016.

[20] J. Hervás *et al.*, "Microwave photonics for optical sensors," *IEEE J. Sel. Topics Quantum Electron.*, vol. 23, no. 2, pp. 327–339, Apr. 2017.

[21] M. E. Froggatt and J. Moore, "High-spatial-resolution distributed strain measurement in optical fiber with Rayleigh scatter," *Appl. Opt.*, vol. 37, no. 10, pp. 1735–1740, 1998.

[22] D. K. Gifford *et al.*, "Swept-wavelength interferometric interrogation of fiber Rayleigh scatter for distributed sensing applications," *Proc. SPIE Fiber Opt. Sensors Appl.*, vol. 6770, Oct. 2007, Art. no. 67700F.

[23] M. Gagné, S. Loranger, J. Lapointe, and R. Kashyap, "Fabrication of high quality, ultra-long fiber Bragg gratings: Up to 2 million periods in phase," *Opt. Express*, vol. 22, no. 1, pp. 387–398, 2014.

[24] *ITU-T G.652: Characteristics of a Single-Mode Optical Fibre and Cable*. Accessed: Jun. 26, 2020. [Online]. Available: https://www.itu.int/rec/T-REC-G.652/en

[25] G. Agrawal, *Applications of Nonlinear Fiber Optics*. Amsterdam, The Netherlands: Elsevier, 2001.

[26] T. Ayupova *et al.*, "Fiber optic refractive index distributed multi-sensors by scattering-level multiplexing with MgO nanoparticle-doped fibers," *IEEE Sensors J.*, vol. 20, no. 5, pp. 2504–2510, Mar. 2020.

[27] S. Korganbayev *et al.*, "Refractive index sensor by interrogation of etched MgO nanoparticle-doped optical fiber signature," *IEEE Photon. Technol. Lett.*, vol. 31, no. 15, pp. 1253–1256, Aug. 1, 2019.

[28] A. Beisenova, A. Issatayeva, I. Iordachita, W. Blanc, C. Molardi, and D. Tosi, "Distributed fiber optics 3D shape sensing by means of high scattering NP-doped fibers simultaneous spatial multiplexing," *Opt. Express*, vol. 27, no. 16, pp. 22074–22087, 2019.

[29] A. Beisenova, A. Issatayeva, S. Korganbayev, C. Molardi, W. Blanc, and D. Tosi, "Simultaneous distributed sensing on multiple MgO-doped high scattering fibers by means of scattering-level multiplexing," *J. Lightw. Technol.*, vol. 37, no. 13, pp. 3413–3421, Jul. 1, 2019.

[30] A. Beisenova *et al.*, "Multi-fiber distributed thermal profiling of minimally invasive thermal ablation with scattering-level multiplexing in MgO-doped fibers," *Biomed. Opt. Express*, vol. 10, no. 3, pp. 1282–1296, 2019.

[31] M. Sypabekova *et al.*, "Fiber optic refractive index sensors through spectral detection of Rayleigh backscattering in a chemically etched MgO-based nanoparticle-doped fiber," *Opt. Lett.*, vol. 43, no. 24, pp. 5945–5948, 2018.

[32] C. Molardi *et al.*, "Fiber Bragg grating (FBG) sensors in a high-scattering optical fiber doped with MgO nanoparticles for polarization-dependent temperature sensing," *Appl. Sci.*, vol. 9, no. 15, p. 3107, Aug. 2019.

[33] A. Yan *et al.*, "Distributed optical fiber sensors with ultrafast laser enhanced Rayleigh backscattering profiles for real-time monitoring of solid oxide fuel cell operations," *Sci. Rep.*, vol. 7, no. 1, Aug. 2017, Art. no. 9360.

[34] S. Loranger, M. Gagné, V. Lambin-Iezzi, and R. Kashyap, "Rayleigh scatter based order of magnitude increase in distributed temperature and strain sensing by simple UV exposure of optical fibre," *Sci. Rep.*, vol. 5, no. 1, Sep. 2015, Art. no. 11177.

[35] F. Parent *et al.*, "Intra-arterial image guidance with optical frequency domain reflectometry shape sensing," *IEEE Trans. Med. Imag.*, vol. 38, no. 2, pp. 482–492, Feb. 2019.

[36] F. Parent *et al.*, "Enhancement of accuracy in shape sensing of surgical needles using optical frequency domain reflectometry in optical fibers," *Biomed. Opt. Express*, vol. 8, no. 4, pp. 2210–2221, 2017.

[37] F. Monet, S. Loranger, V. Lambin-Iezzi, A. Drouin, S. Kadoury, and R. Kashyap, "The ROGUE: A novel, noise-generated random grating," *Opt. Express*, vol. 27, no. 10, pp. 13895–13909, 2019.

[38] D. Tosi, C. Molardi, W. Blanc, T. Paixáo, P. Antunes, and C. Marques, "Performance analysis of scattering-level multiplexing (SLMux) in distributed fiber-optic backscatter reflectometry physical sensors," *Sensors*, vol. 20, no. 9, p. 2595, May 2020.

[39] J. J. Bos, A. K. Sang, M. E. Froggatt, and D. K. Gifford, "Mode conditioner and portable high-resolution reflectometer for maintenance and diagnostics of single and multi-mode avionic fiber networks," in *Proc. IEEE Avionics, Fiber- Opt. Photon. Technol. Conf.*, Oct. 2011, pp. 69–70.

[40] S. Zhang, W. Ji, X. Li, K. Huang, and R. Yin, "Precise failure location and protection mechanism in long-reach passive optical network," *J. Lightw. Technol.*, vol. 34, no. 22, pp. 5175–5182, Nov. 15, 2016.

[41] X. Yi, T. X. H. Huang, and R. A. Minasian, "Tunable and reconfigurable photonic signal processor with programmable all-optical complex coefficients," *IEEE Trans. Microw. Theory Techn.*, vol. 58, no. 11, pp. 3088–3093, Nov. 2010.

[42] J. Sancho *et al.*, "Integrable microwave filter based on a photonic crystal delay line," *Nature Commu.*, vol. 3, no. 1, pp. 1–9. 2012.

[43] I. Gasulla, D. Barrera, J. Hervás, and S. Sales, "Spatial division multiplexed microwave signal processing by selective grating inscription in homogeneous multicore fibers," *Sci. Rep.*, vol. 7, no. 1, Jan. 2017, Art. no. 41727.

[44] L. Gan *et al.*, "Spatial-division multiplexed Mach–Zehnder interferometers in heterogeneous multicore fiber for multiparameter measurement," *IEEE Photon. J.*, vol. 8, no. 1, Feb. 2016, Art. no. 7800908.

[45] R. G. H. van Uden *et al.*, "Ultra-high-density spatial division multiplexing with a few-mode multicore fibre," *Nature Photon.*, vol. 8, no. 11, pp. 865–870, Nov. 2014.

[46] I. Floris, J. Madrigal, S. Sales, P. A. Calderón, and J. M. Adam, "Twisting measurement and compensation of optical shape sensor based on spun multicore fiber," *Mech. Syst. Signal Process.*, vol. 140, Jun. 2020, Art. no. 106700.

[47] F. T. Ulaby, E. Michielssen, and U. Ravaioli, *Fundamentals of Applied Electromagnetics 6E*. Boston, MA, USA: Prentice-Hall, 2010.

[48] M. Froggatt, "Distributed measurement of the complex modulation of a photoinduced Bragg grating in an optical fiber," *Appl. Opt.*, vol. 35, no. 25, pp. 5162–5164, Sep. 1996.

[49] M. D. Mermelstein, R. Posey, G. A. Johnson, and S. T. Vohra, "Rayleigh scattering optical frequency correlation in a single-mode optical fiber," *Opt. Lett.*, vol. 26, no. 2, pp. 58–60, Jan. 2001.

[50] W. Blanc, C. Guillermier, and B. Dussardier, "Composition of nanoparticles in optical fibers by secondary ion mass spectrometry," *Opt. Mater. Express*, vol. 2, no. 11, pp. 1504–1510, 2012.

[51] W. Blanc *et al.*, "Fabrication of rare Earth-doped transparent glass ceramic optical fibers by modified chemical vapor deposition," *J. Amer. Ceram. Soc.*, vol. 94, no. 8, pp. 2315–2318, Aug. 2011.

[52] W. Blanc and B. Dussardier, "Formation and applications of nanoparticles in silica optical fibers," *J. Opt.*, vol. 45, no. 3, pp. 247–254, Sep. 2016.

[53] S. Tammela, M. Söderlund, J. Koponen, V. Philippov, and P. Stenius, "The potential of direct nanoparticle deposition for the next generation of optical fibers," *Proc. SPIE Opt. Compon. Mater.*, vol. 6116, Apr. 2006, Art. no. 61160G.

[54] J. Thomas *et al.*, "Radiation-resistant erbium-doped-nanoparticles optical fiber for space applications," *Opt. Express*, vol. 20, no. 3, pp. 2435–2444, Jan. 2012.

[55] V. Resta *et al.*, "Nanoparticle-doped electrospun fiber random lasers with spatially extended light modes," *Opt. Express*, vol. 25, no. 20, pp. 24604–24614, 2017.

[56] M. J. F. Digonnet, *Rare-Earth-Doped Fiber Lasers and Amplifiers*. Boca Raton, FL, USA: CRC Press, 2001.

[57] R. Chen *et al.*, "Regenerated distributed Bragg reflector fiber lasers for high-temperature operation," *Opt. Lett.*, vol. 38, no. 14, pp. 2490–2492, 2013.

[58] F. Monet, V. Lambin-Iezzi, J. S. Boisvert, B. Maubois, and R. Kashyap, "ROGUE-based, random distributed feedback lasers," *Proc. SPIE Fiber Lasers Technol. Syst.*, vol. 11260, Jul. 2020, Art. no. 112601J.

[59] A. Kersey *et al.*, "Fiber grating sensors," *J. Lightw. Technol.*, vol. 15, no. 8, pp. 1442–1463, Aug. 1997.

[60] S. J. Mihailov, "Fiber Bragg grating sensors for harsh environments," *Sensors*, vol. 12, no. 2, pp. 1898–1918, Feb. 2012.

[61] P. Saccomandi, E. Schena, and S. Silvestri, "Techniques for temperature monitoring during laser-induced thermotherapy: An overview," *Int. J. Hyperthermia*, vol. 29, no. 7, pp. 609–619, Nov. 2013.

[62] E. Schena *et al.*, "Solutions to improve the outcomes of thermal treatments in oncology: Multipoint temperature monitoring," *IEEE J. Electromagn., RF Microw. Med. Biol.*, vol. 2, no. 3, pp. 172–178, Sep. 2018.

[63] E. Schena, D. Tosi, P. Saccomandi, E. Lewis, and T. Kim, "Fiber optic sensors for temperature monitoring during thermal treatments: An overview," *Sensors*, vol. 16, no. 7, p. 1144, Jul. 2016.

[64] S. A. SaPareto and W. C. Dewey, "Thermal dose determination in cancer therapy," *Int. J. Radiat. Oncol. Biol. Phys.*, vol. 10, no. 6, pp. 787–800, Apr. 1984.

[65] H. Rhim *et al.*, "Essential techniques for successful radio-frequency thermal ablation of malignant hepatic tumors," *Radiographics*, vol. 21, pp. 17–35, Oct. 2001.
[66] N. Todd, M. Diakite, A. Payne, and D. L. Parker, "*In vivo* evaluation of multi-echo hybrid PRF/T1 approach for temperature monitoring during breast MR-guided focused ultrasound surgery treatments," *Magn. Reson. Med.*, vol. 72, no. 3, pp. 793–799, Sep. 2014.
[67] V. Rieke, "MR thermometry," in *Interventional Magnetic Resonance Imaging*. Berlin, Germany: Springer, 2011, pp. 271–288.
[68] *ISO 10993-1:2018 Biological Evaluation of Medical Devices*. Accessed: Jun. 26, 2020. [Online]. Available: https://www.iso.org/standard/68936.html
[69] A. A. Issatayeva *et al.*, "Multiplexing of distributed temperature sensing achieved by nanoparticle-doped fibers," *Proc. SPIE Opt. Health Care Biomed. Opt.*, vol. 11190, Jan. 2019, Art. no. 111900H.
[70] M. Jelbuldina *et al.*, "Multi-fiber distributed temperature profiling in ex vivo magnetite nanoparticle-mediated laser tissue ablation," in *Proc. SPIE Opt. Interact. Issue Cells*, vol. 11238, May 2020, Art. no. 112380H.
[71] A. Issatayeva *et al.*, "2D temperature sensing obtained by multiplexing of optical backscattering reflectometry," *Proc. SPIE Opt. Fibers Sensors Med. Diag. Treatment Appl.*, vol. 11233, Apr. 2020, Art. no. 112330T.
[72] A. Beisenova, A. Issatayeva, D. Tosi, and C. Molardi, "Fiber-optic distributed strain sensing needle for real-time guidance in epidural anesthesia," *IEEE Sensors J.*, vol. 18, no. 19, pp. 8034–8044, Oct. 2018.
[73] B. Carotenuto *et al.*, "Optical guidance systems for epidural space identification," *IEEE J. Sel. Topics Quantum Electron.*, vol. 23, no. 2, pp. 371–379, Mar. 2017.
[74] S. Ambastha, S. Umesh, S. Dabir, and S. Asokan, "Spinal needle force monitoring during lumbar puncture using fiber Bragg grating force device," *J. Biomed. Opt.*, vol. 21, no. 11, Nov. 2016, Art. no. 117002.
[75] T. Dhansura, T. Shaikh, M. Maadoo, and F. Chittalwala, "Identification of the epidural space-loss of resistance to saline: An inexpensive modification," *Indian J. Anaesthesia*, vol. 59, no. 10, pp. 677–679, Oct. 2015.
[76] K. Arendt and S. Segal, "Why epidurals do not always work," *Obstetrics Gynecol.*, vol. 1, no. 2, pp. 49–55, 2008.
[77] A. M. Okamura, C. Simone, and M. D. O'Leary, "Force modeling for needle insertion into soft tissue," *IEEE Trans. Biomed. Eng.*, vol. 51, no. 10, pp. 1707–1716, Oct. 2004.
[78] F. Khan, A. Denasi, D. Barrera, J. Madrigal, S. Sales, and S. Misra, "Multi-core optical fibers with Bragg gratings as shape sensor for flexible medical instruments," *IEEE Sensors J.*, vol. 19, no. 14, pp. 5878–5884, Jul. 2019.
[79] A. B. Socorro-Leránoz, D. Santano, I. Del Villar, and I. R. Matias, "Trends in the design of wavelength-based optical fibre biosensors (2008–2018)," *Biosensors Bioelectron.*, vol. 1, Jun. 2019, Art. no. 100015.
[80] A. Iadicicco, A. Cusano, S. Campopiano, A. Cutolo, and M. Giordano, "Thinned fiber Bragg gratings as refractive index sensors," *IEEE Sensors J.*, vol. 5, no. 6, pp. 1288–1295, Dec. 2005.
[81] A. Iadicicco, S. Campopiano, A. Cutolo, M. Giordano, and A. Cusano, "Nonuniform thinned fiber Bragg gratings for simultaneous refractive index and temperature measurements," *IEEE Photon. Technol. Lett.*, vol. 17, no. 7, pp. 1495–1497, Jul. 2005.
[82] S. Gao *et al.*, "High-sensitivity DNA biosensor based on microfiber Sagnac interferometer," *Opt. Express*, vol. 25, no. 12, pp. 13305–13313, 2017.
[83] X. D. Hoa, A. G. Kirk, and M. Tabrizian, "Enhanced SPR response from patterned immobilization of surface bioreceptors on nano-gratings," *Biosensors Bioelectron.*, vol. 24, no. 10, pp. 3043–3048, Jun. 2009.
[84] C. Caucheteur, Y. Shevchenko, L.-Y. Shao, M. Wuilpart, and J. Albert, "High resolution interrogation of tilted fiber grating SPR sensors from polarization properties measurement," *Opt. Express*, vol. 19, no. 2, pp. 1656–1664, 2011.
[85] A. K. Sharma, R. Jha, and B. D. Gupta, "Fiber-optic sensors based on surface plasmon resonance: A comprehensive review," *IEEE Sensors J.*, vol. 7, no. 8, pp. 1118–1129, Aug. 2007.
[86] M. Sypabekova, A. Aitkulov, W. Blanc, and D. Tosi, "Reflector-less nanoparticles doped optical fiber biosensor for the detection of proteins: Case thrombin," *Biosensors Bioelectron.*, vol. 165, Oct. 2020, Art. no. 112365.
[87] M. Sypabekova *et al.*, "Functionalized etched tilted fiber Bragg grating aptasensor for label-free protein detection," *Biosensors Bioelectron.*, vol. 146, Dec. 2019, Art. no. 111765.
[88] A. Morana *et al.*, "Radiation-hardened fiber Bragg grating based sensors for harsh environments," *IEEE Trans. Nucl. Sci.*, vol. 64, no. 1, pp. 68–73, Jan. 2017.
[89] K. Krebber, H. Henschel, and U. Weinand, "Fibre Bragg gratings as high dose radiation sensors?" *Meas. Sci. Technol.*, vol. 17, no. 5, pp. 1095–1102, May 2006.
[90] A. F. Fernandez *et al.*, "Long-term radiation effects on fibre Bragg grating temperature sensors in a low flux nuclear reactor," *Meas. Sci. Technol.*, vol. 15, no. 8, pp. 1506–1511, Aug. 2004.
[91] P. Niay *et al.*, "Behavior of Bragg gratings, written in germanosilicate fibers, against gamma-ray exposure at low dose rate," *IEEE Photon. Technol. Lett.*, vol. 6, no. 11, pp. 1350–1352, Nov. 1994.
[92] M. Olivero *et al.*, "Preliminary investigation of radiation dose sensors based on aluminum-doped silicate optical fibers," in *Proc. IEEE Int. Symp. Med. Meas. Appl. (MeMeA)*, Jun. 2020, pp. 1–5.

Daniele Tosi received the B.Sc. and M.Sc. degrees in telecommunication engineering and the Ph.D. degree in electrical and computer engineering from the Politecnico di Torino in 2004, 2006, and 2010, respectively. He is an Associate Professor of Electrical and Computer Engineering with Nazarbayev University and the Head of the Laboratory of Biosensors and Bioinstruments and the National Laboratory Astana. His research interests include optical fiber sensors, biomedical sensors, distributed sensing, and biosensors. He was a recipient of the IEEE Sensors Council Early Career Technical Award in 2018. He is an Associate Editor of the IEEE SENSORS JOURNAL.

Carlo Molardi (Member, IEEE) received the master's degree in telecommunication engineering and the Ph.D. degree in information technologies from the University of Parma in March 2011 and 2016, respectively. He is working on numerical methods for optics and electromagnetism. He is an Assistant Professor of Electrical and Computer Engineering with Nazarbayev University. He has covered a postdoctoral position at the Information Engineering Department, University of Parma. His research interests include photonic crystal fibers design, fiber lasers for high-power operations, random lasers, fiber optics, fiber sensors, and computational electromagnetism.

Marzhan Sypabekova received the B.Sc. degree in biotechnology from the University of Glasgow, Glasgow, U.K., in 2011, the M.Sc. degree in bionanophotonics from the École Normale Supérieure de Cachan, Paris, France, in 2014, and the Ph.D. degree in science engineering and technology from Nazarbayev University, Nur-Sultan, Kazakhstan, in 2019. Her research interests include optical fiber sensors, biosensors, molecular and cellular biology, and bioengineering. She was recipient of the IEEE Sensors Council and the British Council Travel Grants.

Wilfried Blanc received the M.Sc. and Ph.D. degrees in physics from Claude Bernard University Lyon 1, Lyon, France, in 1996 and 2000, respectively. He held a postdoctoral position at the ICMCB Laboratory, University of Bordeaux, funded by Rhodia S.A. and Solvay S.A. In 2002, he commenced with the Centre National de la Recherche Scientifique (CNRS) at the Laboratoire de Physique de la Matière Condensée (now Institut de Physique de Nice), where his main research interests include the design, realization, and characterization of rare-earth-doped silica optical fibers which are made by using modified chemical vapor deposition (MCVD) technique.